ACS Catalysis

Research Article

Cite This: ACS Catal. 2018, 8, 11377−11385

pubs.acs.org/acscatalysis

Sodium Enhances Ir/TiO_2 Activity for Catalytic Oxidation of Formaldehyde at Ambient Temperature

Yaobin Li,[†,‡,⊥] Xueyan Chen,[†,§,⊥] Chunying Wang,[‡,§] Changbin Zhang,[*,†,§] and Hong He[†,‡,§]

[†]State Key Joint Laboratory of Environment Simulation and Pollution Control, Research Center for Eco-environmental Sciences, Chinese Academy of Sciences, Beijing 100085, China

[‡]Center for Excellence in Regional Atmospheric Environment, Institute of Urban Environment, Chinese Academy of Sciences, Xiamen 361021, China

[§]University of Chinese Academy of Sciences, Beijing 100049, China

Supporting Information

ABSTRACT: The development of highly efficient catalysts for ambient formaldehyde (HCHO) destruction is of great interest for indoor air purification. Here, we show that a sodium (Na)-doped iridium (Ir) catalyst (Ir/TiO_2) is a highly active catalyst for the catalytic oxidation of HCHO at room temperature. We observed that Na addition dramatically enhanced the activity of the Ir/TiO_2-R catalyst, and 100% HCHO conversion was achieved over Na-Ir/TiO_2-R catalyst at a gas hourly space velocity of 100,000 h^{-1} and HCHO inlet concentration of 120 ppm at 25 °C. The Ir/TiO_2 and Na-Ir/TiO_2 catalysts were characterized using X-ray powder diffraction, Brunauer−Emmett−Teller surface area testing, high-angle annular dark-field scanning transmission electron microscopy, H_2 temperature-programmed reduction (TPR), X-ray absorption fine structure, X-ray photoelectron spectroscopy, and CO-TPR. The characterization results show that the addition of Na species had no influence on Ir dispersion on the TiO_2 surface but greatly promoted the activation of both chemisorbed oxygen and H_2O. The reaction mechanism of HCHO oxidation was investigated by using in situ diffuse reflectance infrared transform spectroscopy. The results show that the reaction mechanisms on Ir/TiO_2-R and Na-Ir/TiO_2-R both followed the direct formate oxidation pathway (HCHO → HCOO + OH → CO_2 + H_2O), and the activated oxygen species mainly participated in the formate formation step while the activated OH groups were primarily responsible for the subsequent formate oxidation. Because of the improved capacities for the activation of oxygen and H_2O induced by Na addition, the Na-Ir/TiO_2 catalyst demonstrated much better performance than Ir/TiO_2 for ambient HCHO oxidation.

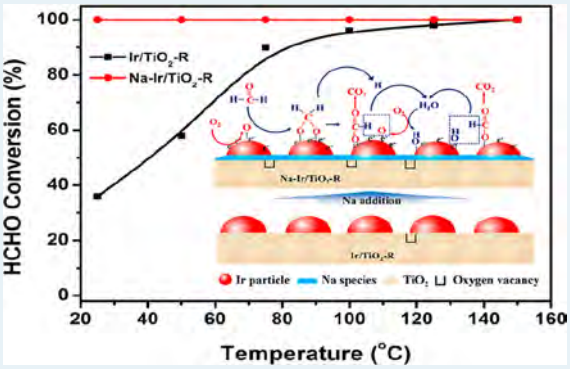

KEYWORDS: *indoor air pollution, Ir-based catalyst, alkali metal, hydroxyl, promotion effect*

1. INTRODUCTION

With increasing concern about indoor air pollution, improving indoor air quality is becoming a critical issue, especially in China.[1] As a major indoor air pollutant, formaldehyde (HCHO) is known to cause irritation of the eyes, skin, and respiratory system and even has carcinogenic effects.[2,3] Therefore, effective abatement of HCHO is of great importance for improving indoor air quality and reducing public health risks.

Several methods have been applied for the removal of HCHO, including adsorption, photocatalysis, plasma technology, and catalytic oxidation.[4−9] Adsorption is the most widely used method for indoor air HCHO removal, but it suffers from limited adsorption capacities of absorbents and secondary pollution during regeneration.[5] Because HCHO can be completely oxidized to form H_2O and CO_2 by catalytic oxidation without other byproducts, this method is now regarded as one of the most promising candidate technologies for indoor air HCHO elimination.[7,10] Transition metal oxides (Co, Ni, Ag, and Mn)[11−16] and supported noble metal (Pt, Pd, Rh, and Au) catalysts[17−27] have been widely investigated for HCHO oxidation. Generally, the transition metal oxides require high temperatures (>100 °C) to achieve complete oxidation of HCHO. In contrast, the supported noble metal catalysts, especially Pt-, Pd-, and Au-based catalysts, exhibit excellent activity for catalytic oxidation of HCHO at ambient temperature without any energy input[23,26,28,29] and are promising for wide application in indoor air HCHO destruction.

We previously reported that Pt/TiO_2 is a highly efficient catalyst for the catalytic oxidation of HCHO.[22,28,30] We also found that alkali ions (such as Li^+, Na^+, and K^+) have a

Received: July 31, 2018
Revised: October 18, 2018
Published: October 25, 2018

DOI: 10.1021/acscatal.8b03026
ACS Catal. 2018, 8, 11377−11385

Table 1. Bulk Composition, Specific Surface Area (BET), Average Pore Size (d_p) and Total Pore Volume (V) of the TiO_2, Na-TiO_2, Ir/TiO_2-R, and Na-Ir/TiO_2-R Catalysts Together with Ir Dispersion (D), Metal Size (d_m), and Turnover Frequencies (TOFs) at 25 °C on the Ir/TiO_2-R and Na-Ir/TiO_2-R Catalysts

	bulk composition (wt %)[a]							
sample	Ir	Na	BET (m^2/g)	d_p (nm)	V (cm^3/g)	d_m[b] (nm)	D[c]	TOFs ($\times 10^{-2}$ s^{-1})
TiO_2			60.8	30.2	0.46			
Na/TiO_2		1.98	54.7	33.4	0.44			
Ir/TiO_2-R	0.99		60.2	30.1	0.45	1.3	69.1%	0.54
Na-Ir/TiO_2-R	0.95	1.95	52.1	34.2	0.45	1.1	81.6%	1.04

[a]Bulk composition was measured by ICP-OES. [b]Measured by HAADF-STEM (100 particles counted). [c]The detail calculation of Ir dispersion is shown in Figure S2.

dramatic promotion effect on the Pt/TiO_2 catalyst by inducing and stabilizing atomically dispersed Pt species.[29] Recently, researchers demonstrated that the alkali metal-promotion effect for Pt is also manifested for Pd-/Ag-based and even HMO catalysts.[31−33] Iridium (Ir) is another platinum group metal that can be well-dispersed on some supports.[34] However, compared with Pt-, Au-, and Pd-based catalysts, Ir-based catalysts have been less investigated in heterogeneous catalysis and have not yet been studied for the HCHO oxidation reaction. In addition, because Ir has a higher melting point and surface energy than Pt and Pd, it might have a different interaction with alkali ions. Therefore, exploring Ir-based catalysts for HCHO oxidation and determining if alkali ions also have a promotion effect on Ir catalysts are important avenues of research.

In this paper, we prepared Ir/TiO_2 catalysts with and without sodium (Na) addition and tested their catalytic activities for HCHO oxidation at low temperature. It was verified that Na addition had a dramatic promotion effect on the Ir-based catalyst. Na-Ir/TiO_2-R catalyst showed much higher performance for ambient HCHO oxidation than that of the Na-free catalyst, achieving 100% conversion of 120 ppm of HCHO to CO_2 and H_2O at a gas hourly space velocity (GHSV) of 100,000 h^{-1} at 25 °C. The Ir/TiO_2 and Na-Ir/TiO_2 catalysts were next characterized using X-ray powder diffraction (XRD), Brunauer−Emmett−Teller (BET) surface area testing, high-angle annular dark-field scanning transmission electron microscopy (HAADF-STEM), H_2 temperature-programmed reduction (H_2-TPR), X-ray absorption fine structure (XAFS), X-ray photoelectron spectroscopy (XPS), and in situ diffuse reflectance infrared transform spectroscopy (DRIFTS) methods. On the basis of the characterization results, the Na-promotion mechanism, reaction mechanism, and role of both O_2 and H_2O in HCHO oxidation on Ir-based catalysts were carefully discussed and elucidated.

2. MATERIALS AND METHODS

2.1. Material Preparation. The 1 wt % Ir/TiO_2, 2 wt % Na/TiO_2, and 2 wt % Na/1 wt % Ir/TiO_2 samples were prepared according to previous research.[31] Typically, Na_2CO_3 and iridium acetate (Alfa Aesar) were used for catalyst preparation. After the samples were prereduced using H_2 at 300 °C for 1 h, the catalysts were denoted as TiO_2-R, Na/TiO_2-R, Ir/TiO_2-R, and Na-Ir/TiO_2-R, respectively. The Ir and Na contents in the Ir/TiO_2 and Na-Ir/TiO_2 catalysts were measured by inductively coupled plasma optical emission spectrometry (ICP-OES) (OPTIMA 2000, PerkinElmer), and the results are presented in Table 1. It is shown that the Ir contents were 0.99 and 0.95 wt % on the Ir/TiO_2-R and Na-Ir/TiO_2-R catalysts, respectively; Na contents were 1.98 and 1.95 wt % on the Na/TiO_2 and Na-Ir/TiO_2-R catalysts, respectively.

2.2. Material Characterization. XRD, N_2 adsorption−desorption analysis, HAADF-STEM, and XPS were carried out according to our previous work.[21,31] Before characterization, all samples were pretreated with H_2 at 300 °C for 1 h. H_2-TPR of the fresh Ir/TiO_2 and Na-Ir/TiO_2 samples was carried out according to the previous work,[31] and TPR of Ir/TiO_2-R and Na-Ir/TiO_2-R catalysts followed the same procedure as in another previous work.[21]

The in situ XANES spectra of the Ir−L_{III} edges of the Ir/TiO_2 and Na-Ir/TiO_2 samples during reduction by 10% H_2/Ar were collected on the BL14W1 beamline, Shanghai Synchrotron Radiation Facility (SSRF). The reduction temperature was ramped up to 300 °C at a rate of 5 °C/min and then maintained at 300 °C for 1 h in a flow of 10% H_2/Ar (100 mL). The samples were then cooled to room temperature under protection of H_2/Ar after which the gas was switched into N_2 for 30 min and finally to air. Data were analyzed using Athena and Artemis from the Ifeffit 1.2.11 software package. XANES spectra were normalized with the edge height.

2.3. Activity Test for Formaldehyde Oxidation. The activity tests for the catalytic oxidation of HCHO over the catalysts (~60 mg) were performed in a fixed-bed quartz flow reactor with a gas mixture containing 120 ppm of HCHO, 20% O_2, and He balance at a total flow rate of 100 cm^3 min^{-1} (GHSV = 100,000 h^{-1}). All gas streams were humidified to a relative humidity (RH) of ~50%. Turnover frequencies (TOFs) were obtained in a separate experiment where the conversion of HCHO was kept below 30% by varying the inlet HCHO concentration and GHSV with negligible heat and mass-transfer effects. Typically, the samples were tested with 250 ppm inlet HCHO, GHSV of 300000 h^{-1}, and RH of 50% at 25 °C. The TOF calculations followed the same procedure in our previous work.[21] Stability testing and H_2O startup-shutdown cycling were performed under harsher conditions with 200 ppm of HCHO and 200,000 h^{-1} at 25 °C. Analyses of inlet and outlet gases and the carbon balance calculation were performed according to our previous study.[30]

3. RESULTS AND DISCUSSION

3.1. Activity Test. The HCHO oxidation performances of Ir/TiO_2-fresh, Na-Ir/TiO_2-fresh, Ir/TiO_2-R, Na-Ir/TiO_2-R, pure TiO_2-R, and Na/TiO_2-R were evaluated, and the results are presented in Figure S1 and Figure 1, respectively. As shown in Figure S1, both Ir/TiO_2-fresh and Na-Ir/TiO_2-fresh possessed rather poor performances for HCHO oxidation, especially at room temperature. Interestingly, Na-Ir/TiO_2-fresh

DOI: 10.1021/acscatal.8b03026
ACS Catal. 2018, 8, 11377−11385

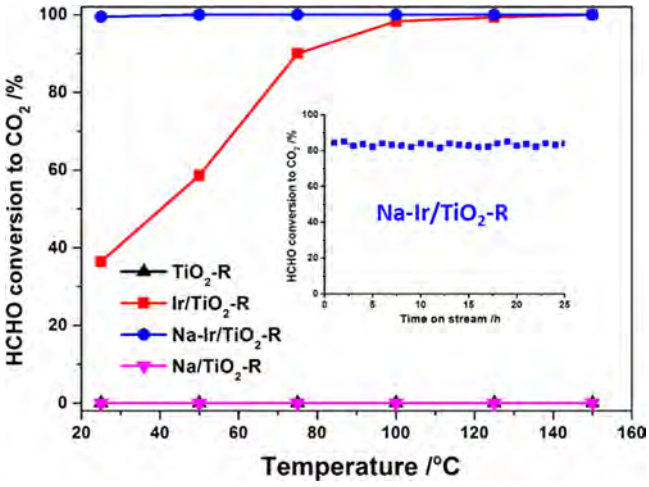

Figure 1. HCHO conversion over TiO_2-R, 2Na/TiO_2-R, Ir/TiO_2-R, and Na-Ir/TiO_2-R samples at different temperatures. Reaction conditions: 120 ppm of HCHO, 20% O_2, 50% RH, He balance, GHSV 100,000 h^{-1} (inset: results of stability testing performed at 25 °C under harsher conditions with 200 ppm of HCHO and 200,000 h^{-1} GHSV).

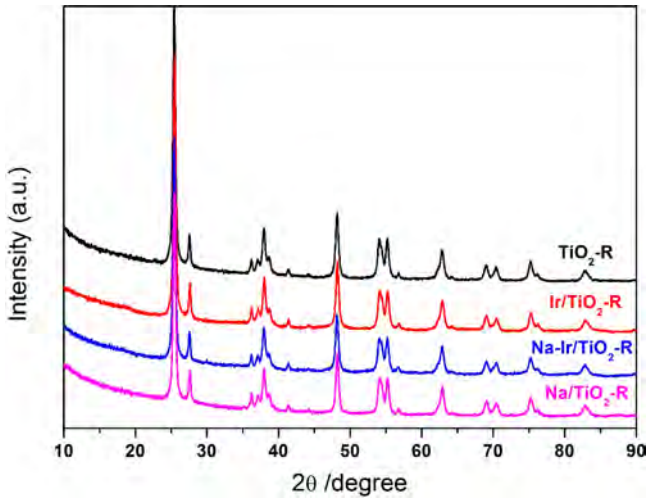

Figure 2. XRD patterns of Ir/TiO_2-R and Na-Ir/TiO_2-R together with TiO_2-R and Na/TiO_2-R samples.

had a higher activity than Ir/TiO_2-fresh. As shown in Figure 1, the performances of the samples were greatly enhanced after H_2 pretreatment, indicating that the metallic Ir species were the active sites for HCHO oxidation on the Ir/TiO_2 system. The Ir/TiO_2-R catalyst presented 36 and 100% HCHO conversion at 25 and 150 °C, respectively. The Na-Ir/TiO_2-R catalyst showed a much higher performance than Ir/TiO_2-R for HCHO oxidation with 100% HCHO conversion to CO_2 at 25 °C under 120 ppm of HCHO and GHSV of 100,000 h^{-1}, demonstrating a dramatic promotion effect of Na addition on Ir/TiO_2-R. Moreover, a long isothermal test at 25 °C was also carried out on the Na-Ir/TiO_2-R catalyst under harsher conditions with 200 ppm inlet HCHO and GHSV of 200,000 h^{-1}. As shown in Figure 1 (inset), the Na-Ir/TiO_2-R catalyst had an excellent stability, and ~80% HCHO conversion was maintained over the 25 h test.

3.2. Structural Features of Catalysts. XRD and BET measurements were carried out to investigate the crystalline structures and physical properties of the samples. Figure 2 shows the XRD patterns of Ir/TiO_2-R and Na-Ir/TiO_2-R together with those of TiO_2 and Na/TiO_2. There were no diffraction peaks of Ir species (Ir^0, IrO_2) in any samples, indicating that Ir species were highly dispersed on the TiO_2 support. As shown in Table 1, the specific surface area, pore diameter, and volume values of Ir/TiO_2-R were similar to those of pure TiO_2-R, whereas the addition of Na somewhat decreased the specific surface area of Ir/TiO_2 due to the loss of small pores covered by the Na species similar to that observed in the Na−Pt/TiO_2 and Na−Pd/TiO_2 systems.[25,31]

3.3. Ir Dispersion and Particle Size on Catalyst. Aberration-corrected HAADF-STEM measurements were performed next to investigate the morphology and particle size distribution of Ir particles on the TiO_2 surface before and after Na addition. The HAADF/STEM images and Ir particle size distribution of Ir/TiO_2-R and Na-Ir/TiO_2-R are shown in Figure 3. Before Na addition, Ir was already highly dispersed on the Ir/TiO_2-R catalyst, and the average Ir particle size (d_m) was 1.3 nm. The Na addition showed no obvious influence on Ir dispersion, and the average Ir particle size on the Na-Ir/TiO_2-R catalyst only decreased slightly to 1.1 nm. We previously found that Na addition to Pt/TiO_2 induced and stabilized atomically dispersed Pt species, and Na addition to Pd/TiO_2 decreased the Pd particle size from 11.4 to 3.4 nm via the strong interaction between Pt/Pd and Na species.[25,31] In contrast, Na addition showed no clear promotion effect on Ir dispersion on TiO_2, which could be ascribed to the different chemical properties of Ir species resulting in different interactions between Ir and TiO_2/Na compared with those of Pt or Pd species.[21]

On the basis of the results of Ir^0 particle size, the Ir dispersions on Ir/TiO_2-R and Na-Ir/TiO_2-R catalysts were calculated following the model and equations in the Supporting Information (Figure S2).[35] The Ir^0 dispersions on Ir/TiO_2-R and Na-Ir/TiO_2-R catalysts were 69.1 and 81.6%, respectively, and the results are shown in Table 1. The TOFs on Ir/TiO_2-R and Na-Ir/TiO_2-R catalysts were next calculated according to the Ir dispersions, and the results are also presented in Table 1. The Ir/TiO_2-R and Na-Ir/TiO_2-R catalysts presented the TOFs of 0.54×10^{-2} and 1.04×10^{-2} s^{-1}, respectively. It is clear that the Na addition significantly enhanced the activity of the Na-Ir/TiO_2-R catalyst with a TOF twice higher than that of the Ir/TiO_2-R catalyst.

3.4. Reducibility of Catalysts. The effect of Na addition on the reducibility of the fresh Ir/TiO_2 and Na-Ir/TiO_2 catalysts was investigated by H_2-TPR measurements, and the results are shown in Figure 4. As shown in Figure 4 (inset), no obvious H_2 consumption was observed on pure TiO_2. Two H_2 consumption peaks at 350−550 °C and >600 °C were presented on fresh Na/TiO_2, which were assigned to the reduction of residual Na_2CO_3 and bulk TiO_2, respectively. There were three H_2 consumption peaks for the Ir/TiO_2-fresh sample. The peak at 140 °C was attributed to the reduction of IrO_2 to Ir; the peak at 220 °C was due to the partial reduction of surface TiO_2 adjacent to Ir sites. The addition of Na to Ir/TiO_2 showed limited influence on the reduction of IrO_2 and bulk TiO_2 but facilitated the reduction of surface TiO_2 adjacent to the Ir sites, shifting the peak to the low temperature range. In addition, the peak appearing at 300−500 °C for Na-Ir/TiO_2-fresh was due to the reduction of residual Na_2CO_3. Compared to the TPR result of fresh Na/TiO_2, the reduction of residual Na_2CO_3 on Na-Ir/TiO_2-fresh was shifted to lower

DOI: 10.1021/acscatal.8b03026
ACS Catal. 2018, 8, 11377−11385

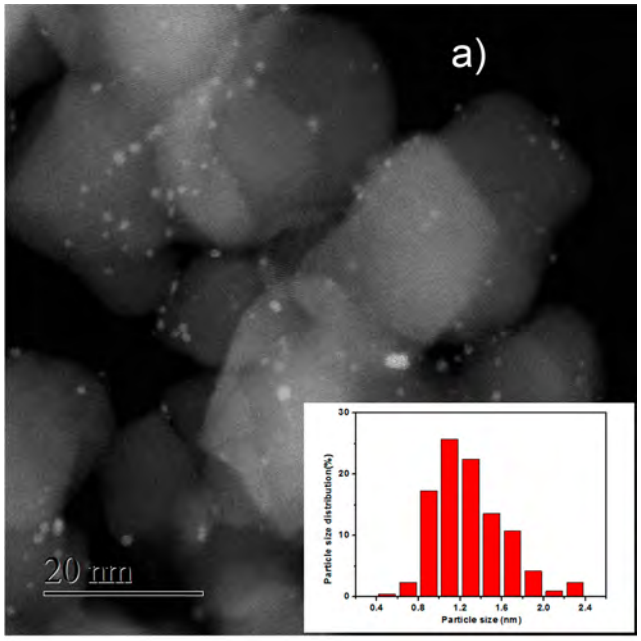

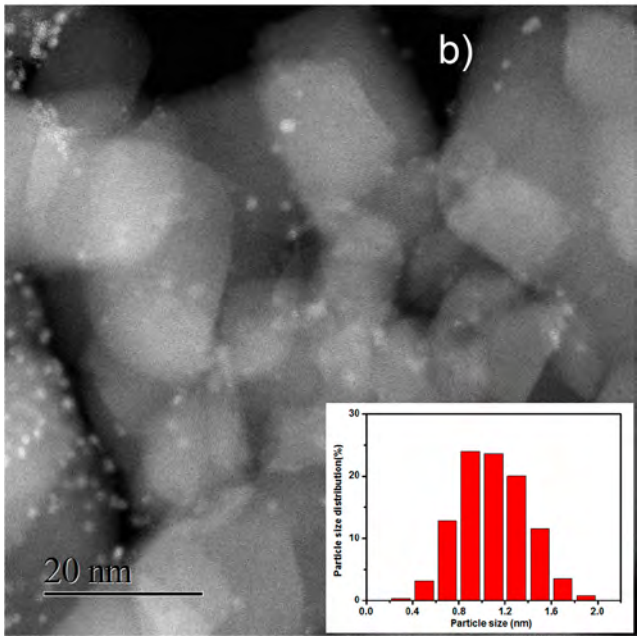

Figure 3. Aberration-corrected HAADF/STEM images and particle size distribution (inset, 100 particles counted) of (a) Ir/TiO_2-R and (b) $Na\text{-}Ir/TiO_2$-R.

temperature, which should be due to the strong interaction between Ir and Na species facilitating the reduction of Na species.

For the capacities of the Ir/TiO_2-R and $Na\text{-}Ir/TiO_2$-R samples to be further investigated for O_2 adsorption and activation at room temperature, second H_2-TPR measurements on the Ir/TiO_2-R and $Na\text{-}Ir/TiO_2$-R catalysts were carried out. The fresh Ir/TiO_2 and $Na\text{-}Ir/TiO_2$ samples were first reduced under H_2 at 300 °C for 1 h followed by purging with helium for 30 min at 300 °C to desorb H_2 and H_2O. After the system was cooled in helium to 25 °C, the gases were switched to 10% O_2/He for 30 min to adsorb and activate O_2 followed by purging with helium for 30 min. The system was next cooled to

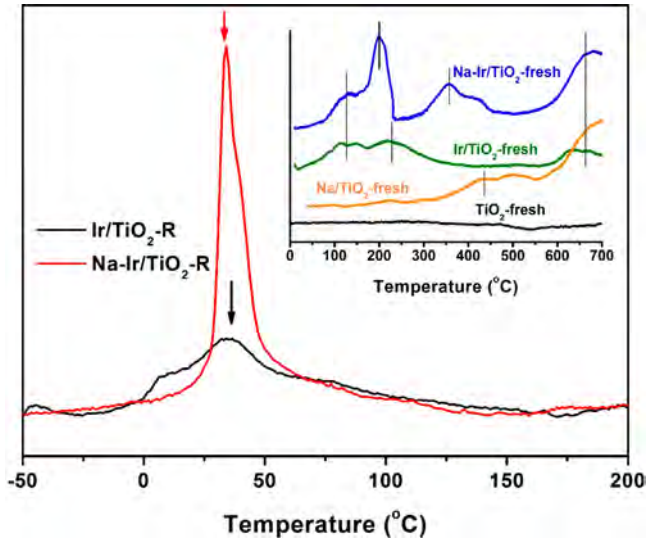

Figure 4. H_2-TPR profiles of fresh Ir/TiO_2, fresh $Na\text{-}Ir/TiO_2$, fresh Na/TiO_2, fresh TiO_2, Ir/TiO_2-R, and $Na\text{-}Ir/TiO_2$-R samples.

−50 °C, and then a second TPR was carried out with 10% H_2/Ar from −50 to 100 °C at a rate of 10 °C/min. As shown in Figure 4, only one peak at 30 °C appeared for the two catalysts, which was attributed to the reduction of chemisorbed oxygen species. Clearly, there was more chemisorbed oxygen on the $Na\text{-}Ir/TiO_2$-R catalyst, indicating that the capacity of Ir/TiO_2-R for O_2 chemisorption and activation was indeed enhanced by Na addition and therefore beneficial to the HCHO oxidation reaction.

3.5. XAFS and XPS Analysis. For understanding the chemical state of the Ir/TiO_2-R catalyst before and after Na addition, XAFS measurements were conducted for Ir/TiO_2 and $Na\text{-}Ir/TiO_2$ before H_2 reduction, after in situ H_2 reduction at atmospheric pressure, and after exposure to air following H_2 reduction. Figure 5 displays the normalized Ir-L_{III} edge XANES spectra and first-order derivatives of the Ir/TiO_2 and $Na\text{-}Ir/TiO_2$ catalysts, IrO_2, and Ir foil. As shown in Figure 5a, the Ir species in both Ir/TiO_2 and $Na\text{-}Ir/TiO_2$ were predominantly in the oxidized state before H_2 reduction, as can be seen by comparing their white line locations and intensities with those of Ir foil and IrO_2. The Ir species were reduced to the metallic state during the in situ reduction (Figure 5b). With further exposure to ambient air (Figure 5c), the Ir species still remained primarily in the metallic state but became partially oxidized, possibly due to the dissociative adsorption of O_2.

The states of the Ir, Ti, and O elements on the catalyst surface were next analyzed by XPS, and the results are shown in Figure 6. Because there is overlap between Ir 4f and Ti 3s, we measured the Ir 4d spectra. As shown in Figure 6a, two Ir $4d_{5/2}$ peaks centered at 296.6 and 296.2 eV appeared on the Ir/TiO_2-R sample, which were assigned to metallic Ir species,[36] and these two peaks shifted to lower energies by 0.4 eV on the $Na\text{-}Ir/TiO_2$-R catalyst. Therefore, we confirmed that electrons were transferred from the Na dopant (electron donor) to Ir^0 species through interaction, leading to the formation of a negatively charged Ir^0 species.[37,38] Furthermore, O_2 adsorption and activation can be enhanced by the formation of negatively charged Ir^0 species through the donation of electrons from a noble metal to the antibonding π^* orbital of O_2,[25,26] which is in line with the results of the H_2-TPR measurements on the reduced samples.

DOI: 10.1021/acscatal.8b03026
ACS Catal. 2018, 8, 11377−11385

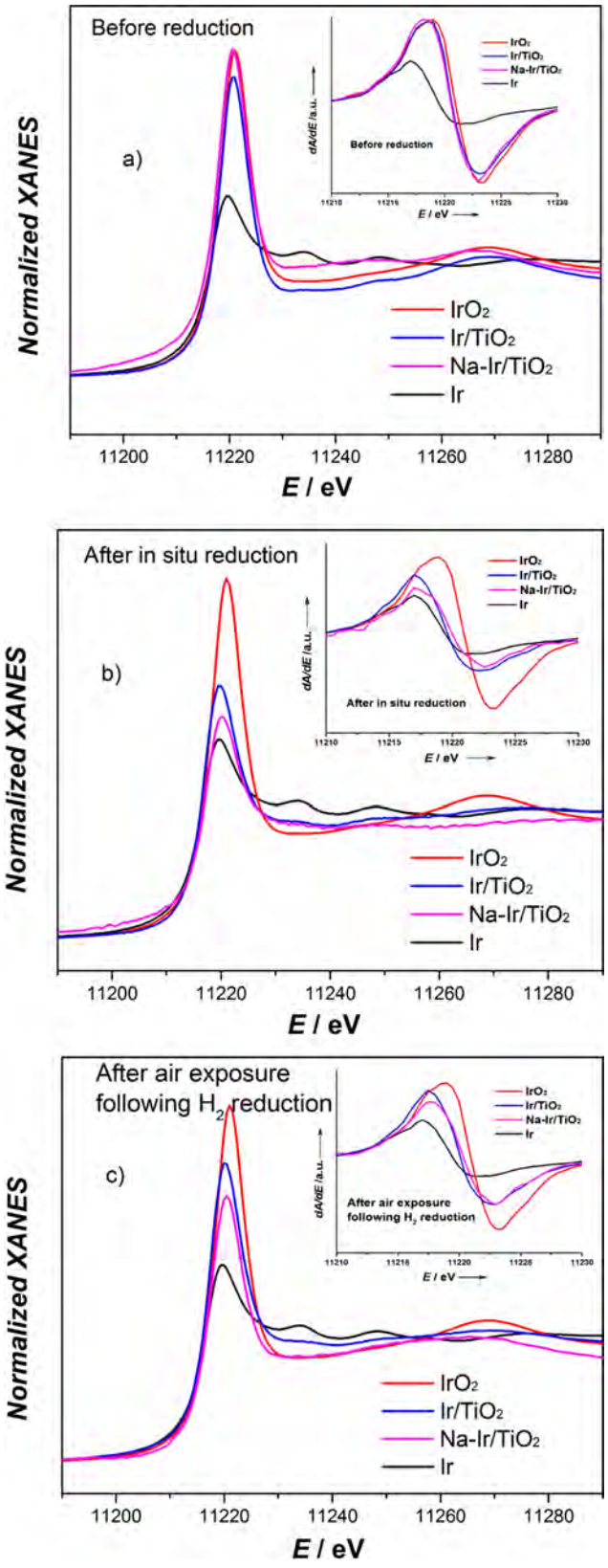

Figure 5. (a) Ir L_{III} edge XANES spectra and first-order derivatives of Ir/TiO_2 and $Na\text{-}Ir/TiO_2$ catalysts before H_2 reduction, (b) after in situ reduction, and (c) after air exposure following H_2 reduction together with those of IrO_2 and Ir foil.

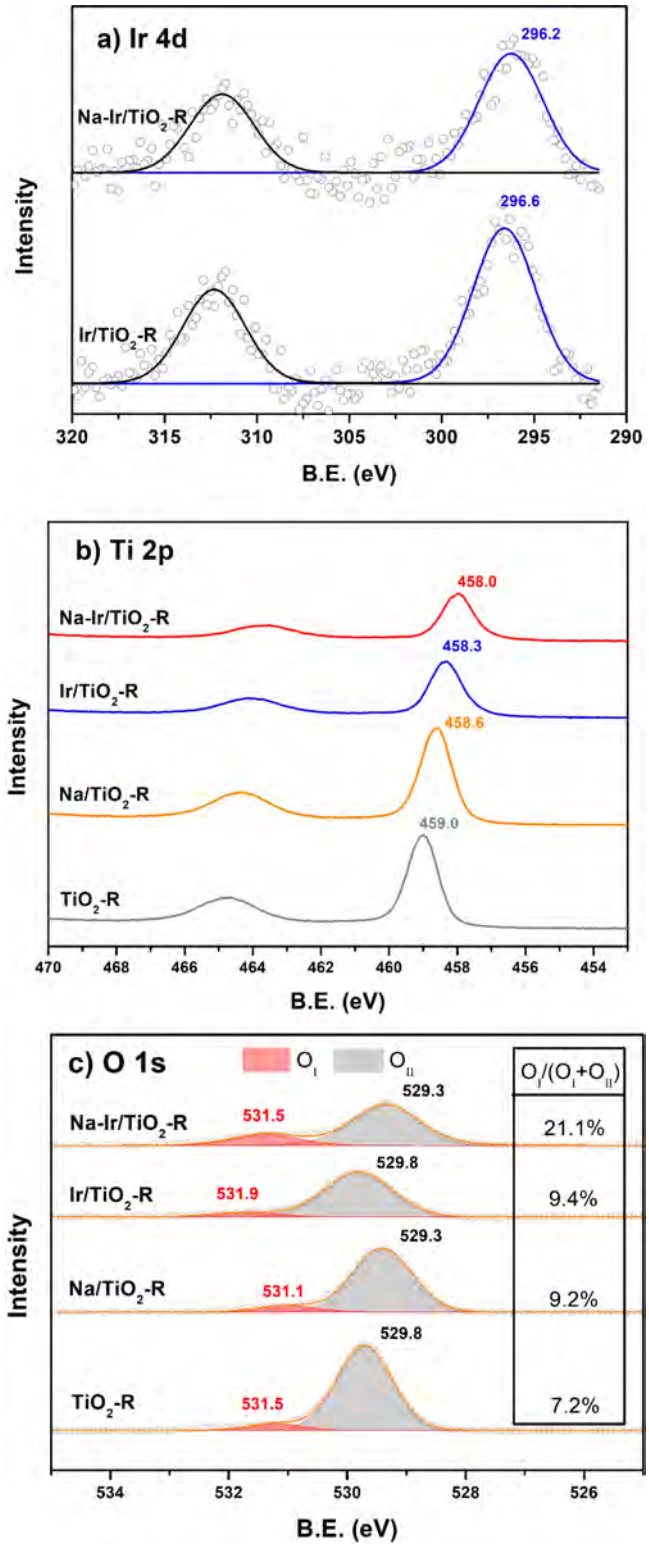

Figure 6. XPS spectra of Ir/TiO_2-R and $Na\text{-}Ir/TiO_2$-R together with TiO_2-R and Na/TiO_2-R samples: (a) Ir 4d, (b) Ti 2p, and (c) O 1s.

Figure 6b shows the Ti 2p peaks of the series of catalysts. The peaks at 458.0−459.0 eV were ascribed to Ti^{4+} of TiO_2.[25] Compared with TiO_2-R, a negative shift of 0.7 eV occurred on the Ir/TiO_2-R samples, which was attributed to the partial reduction of TiO_2 by H_2 spillover on the Ir species during the reduction process. A negative shift of 0.4 eV was also observed on the Na/TiO_2-R catalyst. Likewise, Na addition also induced a slight negative shift of 0.3 eV on the $Na\text{-}Ir/TiO_2$-R catalyst compared with the Ir/TiO_2-R catalyst, indicating that alkali

DOI: 10.1021/acscatal.8b03026
ACS Catal. 2018, 8, 11377−11385

metals may induce the formation of TiO_{2-x} species through interaction with the support,[39,40] and it seems that more TiO_{2-x} species existed on the Na-Ir/TiO_2-R catalyst than on the Ir/TiO_2-R catalyst.

The O 1s XPS spectra of the catalysts are shown in Figure 6c. All samples possessed two kinds of O species. The main peak at the binding energy range of 529.3−529.8 eV was assigned to the lattice oxygen of bulk TiO_2 (O_{II}), and the small shoulder peak in the binding energy range of 530.8−531.5 eV was ascribed to surface chemisorbed hydroxyl species (Ti−OH).[41] The relative contents of Ti−OH on the samples were also estimated. The Ir/TiO_2-R sample possessed only 9.4% Ti−OH, similar to the TiO_2-R and Na/TiO_2-R samples. Remarkably, the relative content of Ti−OH species increased to 21.1% on the Na-Ir/TiO_2-R catalyst, demonstrating that Na addition increased the concentration of surface OH groups. Onishi et al. have shown that Na deposited on TiO_2 (110) strongly interacted with surface oxygen atoms, thereby causing the charge transfer to the substrate followed by reduction of TiO_2 and then forming TiO_{2-x}.[40] TiO_{2-x} is known to facilitate the dissociation of H_2O to form surface OH.[42] In addition, Zhai et al. have reported that alkali metal addition to Pt could significantly enhance the OH binding to form a PtNaOx-(OH)y species, which is beneficial for H_2O activation.[43] The Na addition into Ir/TiO_2 may also induce an IrNaOx(OH)y species, therefore promoting the H_2O activation to surface OH.

We also performed CO-TPR ($2CO + 2OH \rightarrow 2CO_2 + H_2$) to determine whether activation of the surface OH species was enhanced on the Na-promoted Ir/TiO_2 catalyst. As shown in Figure 7, more H_2 and CO_2 were generated on the Na-Ir/

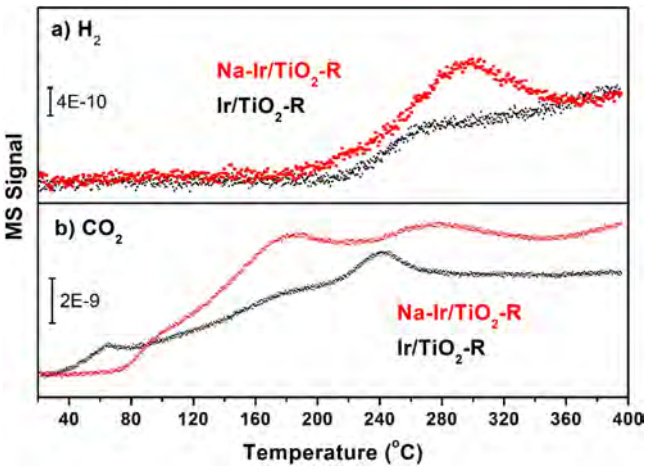

Figure 7. CO-TPR profiles of Ir/TiO_2-R and Na-Ir/TiO_2-R samples.

TiO_2-R catalyst than on the Ir/TiO_2-R catalyst, indicating that more active OH groups existed on the Na-Ir/TiO_2-R catalyst to react with CO to produce CO_2 and H_2. We have previously shown that surface OH groups play an important role in ambient HCHO oxidation because OH reaction with formate species to final products is a facile pathway for HCHO oxidation.[24] Therefore, the enhancement of the surface OH concentration by Na addition is one of the main reasons for the improved performance of Ir/TiO_2-R for HCHO oxidation.

3.6. Role of O_2 and H_2O in HCHO Oxidation. O_2 and H_2O startup-shutdown cycling experiments were next performed to clarify the role of O_2 and H_2O in HCHO oxidation, and the results are shown in Figures 8 and 9. As seen from Figure 8a, the Ir/TiO_2-R catalyst showed almost no

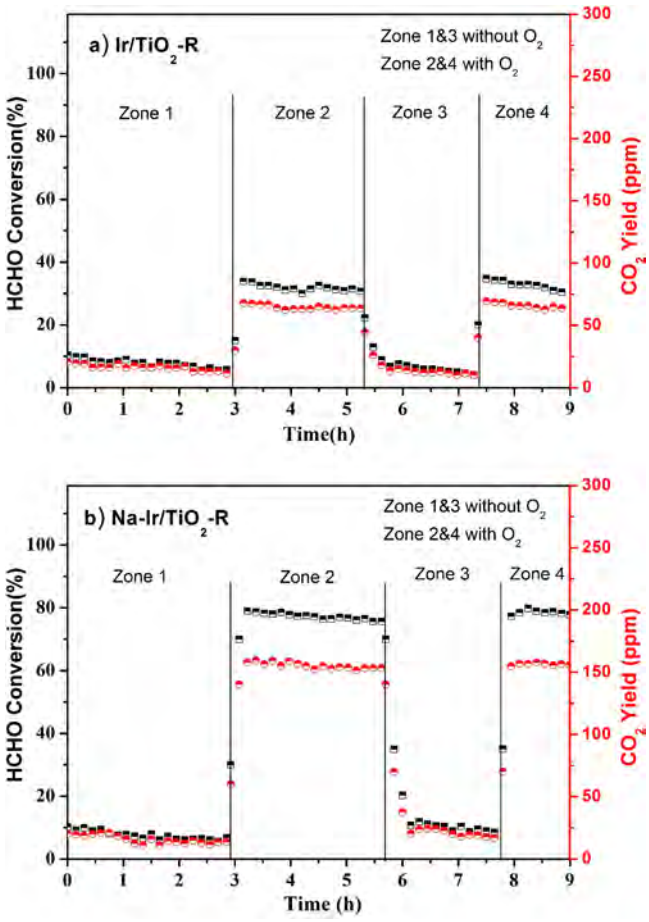

Figure 8. O_2 effect on the activity of (a) Ir/TiO_2-R and (b) Na-Ir/TiO_2-R catalysts (Zones 1 and 3, HCHO + He + H_2O; Zones 2 and 4, HCHO + He + O_2 + H_2O). Reaction conditions: 200 ppm of HCHO, 20% O_2, 50% RH, He balance, 200000 h^{-1} GHSV, 25 °C.

activity for HCHO oxidation at room temperature in the absence of O_2 (Zones 1 and 3), whereas ∼30% HCHO conversion was achieved after introducing O_2 into the flow gases (Zones 2 and 4). A similar phenomenon was also observed for the Na-Ir/TiO_2-R catalyst. When there was no O_2, the Na-Ir/TiO_2-R catalyst was not active for HCHO oxidation. When O_2 was present, the performance of the Na-Ir/TiO_2-R catalyst was greatly enhanced, and HCHO conversion reached ∼80%. As shown in Figure 9, when there was no moisture in the flow gases, the Ir/TiO_2-R catalyst was also not active for HCHO oxidation at room temperature (Zones 1 and 3). After introducing water vapor into the flow gases (Zones 2 and 4), ∼30% HCHO conversion was obtained. The activity of the Na-Ir/TiO_2-R catalyst also depended on the presence of moisture. When there was no moisture, the Na-Ir/TiO_2-R catalyst was not active. However, when water vapor was present, the Na-Ir/TiO_2-R catalyst showed much higher activity than that of the Ir/TiO_2-R catalyst, and ∼80% HCHO conversion could be reached.

The results presented above indicate there was a synergistic effect between H_2O and O_2 in HCHO oxidation, and both of them play an important role in the reaction on Ir/TiO_2-R and Na-Ir/TiO_2-R catalysts at room temperature, which was also

DOI: 10.1021/acscatal.8b03026
ACS Catal. 2018, 8, 11377−11385

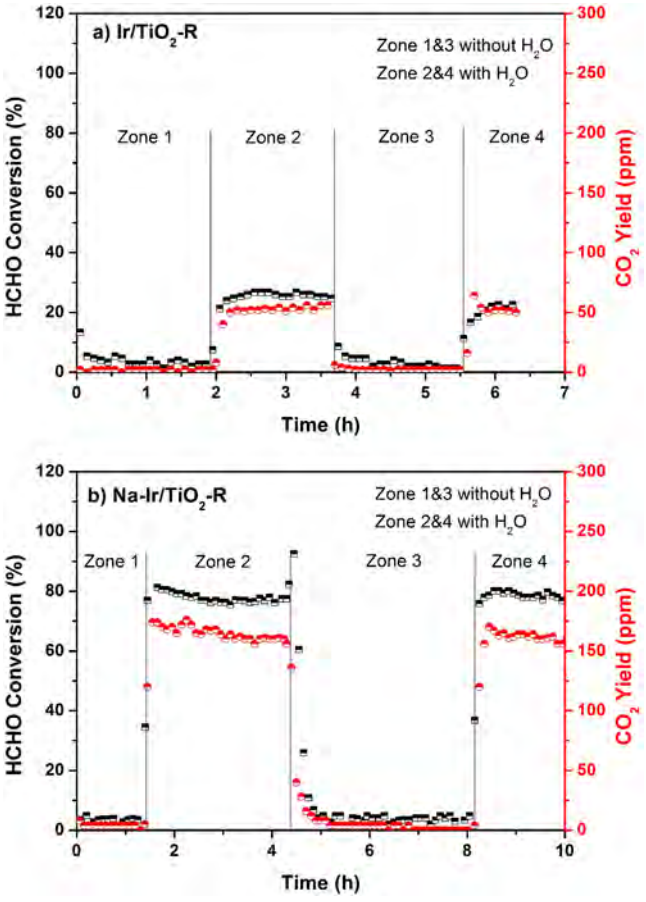

Figure 9. H_2O effect on the activity of the (a) Ir/TiO_2-R and (b) Na-Ir/TiO_2-R catalysts (zone 1 and 3, HCHO+He+O_2; zone 2 and 4, HCHO+He+O_2+H_2O). Reaction conditions: 200 ppm of HCHO, 20% O_2, 50% RH, He balance, GHSV 200,000 h^{-1}, 25 °C.

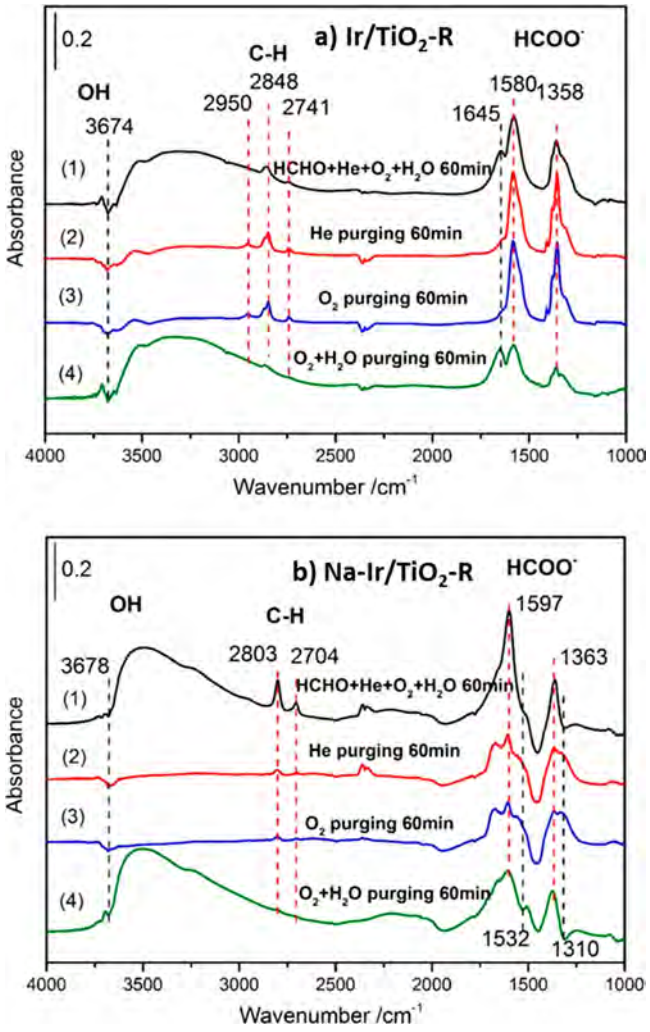

Figure 10. In situ DRIFTS spectra over (a) Ir/TiO_2-R and (b) Na-Ir/TiO_2-R in a flow of He + HCHO + O_2 + H_2O for 60 min (1) followed by He purging for 60 min (2) and O_2 purging for 60 min (3), and finally by O_2 + H_2O purging for 60 min (4) at room temperature. For the dynamic time sequence of the DRIFTS spectra, see Figures S1 and S2. Reaction conditions: 120 ppm of HCHO, 20% O_2, 50% RH, He balance, total flow rate of 100 cm^3 min^{-1}.

demonstrated by DFT calculations.[44,45] It has been reported that surface OH groups are formed by water dissociation on oxygen vacancies[42,46,47] or on metal surfaces through water–oxygen interactions.[48−50] The OH species can also facilitate O_2 adsorption and activation on TiO_2 (110)[25,51] and enhance the diffusion of oxygen.[51,52] Because the Na-Ir/TiO_2-R catalyst possessed a much higher capacity for O_2 and H_2O activation than the Ir/TiO_2-R catalyst, it demonstrated much better performance.

3.7. In Situ DRIFTS Study. The reaction mechanism of HCHO oxidation on Ir/TiO_2-R and Na-Ir/TiO_2-R catalysts was investigated at room temperature by using in situ DRIFTS. The spectra at steady state are presented in Figure 10, and the dynamic DRIFTS spectra with time are given in Figure S3. As shown in Figure 10a, when the Ir/TiO_2-R catalyst was exposed to a flow of HCHO + He + O_2 + H_2O for 60 min, bands at 1358, 1580, 1645, 2741, 2848, and 3674 cm^{-1} appeared. According to previous studies, the bands at 1358 and 1580 cm^{-1} were ascribed to the symmetric stretch ν_s (COO^-) and the asymmetric stretch ν_{as} (COO^-) of formate species, respectively, and the bands at 2741 and 2848 cm^{-1} were related to the ν(C−H) of formate.[28,44,45] A broad absorption band ranging from 3700 to 3000 cm^{-1} and the peak at 1645 cm^{-1} were due to water adsorbed on the catalyst.[44,46] Meanwhile, a negative peak of surface hydroxyl (OH) species at 3674 cm^{-1} was observed on the catalyst surface,[28,46] suggesting that the formation of surface $HCOO^-$ consumed some OH species. There was no peak associated with molecularly adsorbed HCOOH or HCHO on the Ir/TiO_2-R catalyst, indicating that the adsorbed HCHO was rapidly converted to formate species in the flow of HCHO + He + O_2 + H_2O.

The flow of HCHO + O_2 + H_2O was then switched off, and the system was purged by He for 60 min. With helium purging, the broad band ranging from 3700 to 3000 cm^{-1} and the peak at 1645 cm^{-1} dramatically decreased, indicating that a large amount of adsorbed water was removed. The bands of formate species (1358, 1580, 1645, 2741, and 2848 cm^{-1}) were slightly increased, and a very weak band classified as ν(C−H) appeared at 2950 cm^{-1}, which is due to the adsorption of the residual HCHO after the adsorbed water was purged. Upon subsequent exposure of the catalyst to O_2 for 60 min, all peaks basically remained unchanged, demonstrating that oxygen has a limited effect on the decomposition of formate species on the Ir/TiO_2-R catalyst. In contrast, when water vapor was reintroduced into the system, the formate species clearly decreased. These results showed that surface OH

DOI: 10.1021/acscatal.8b03026
ACS Catal. 2018, 8, 11377−11385

groups play an important role in formate oxidation, which was in agreement with the results of H_2O startup-shutdown cycling experiment. As shown in O_2 startup-shutdown results (Figure 8), oxygen was also indispensable for HCHO oxidation because the formation of the formate species is dependent on the presence of O_2.[47] Taking these results into account, we believe that the HCHO oxidation reaction on the Ir/TiO_2 catalyst followed the direct formate oxidation mechanism with the formate oxidation by OH being the rate controlling step.

The same in situ DRIFTS experiments were also performed for the $Na\text{-}Ir/TiO_2\text{-}R$ catalyst. The spectra at steady state are presented in Figure 10b, and the dynamic DRIFTS spectra with time are given in Figure S4. After the samples were exposed to a flow of HCHO + He + O_2 + H_2O for 60 min, formate species (1597, 1363 cm^{-1} for $\nu(COO^-)$ and 2803, 2704 cm^{-1} for $\nu(C-H)$) were formed and were dominant on the catalyst surface. A negative peak of surface hydroxyl (OH) groups at ~3678 cm^{-1} was also observed. With He purging, the peak intensities of the $HCOO^-$ and H_2O bands dropped simultaneously (shown in Figure S4), and the formate species almost disappeared after 60 min. Meanwhile, surface carbonate and bicarbonate species (1310 and 1532 cm^{-1})[28] appeared and gradually increased with formate consumption, indicating that the formate species reacted with active OH groups to generate carbonate or bicarbonate species. Further purging the system with O_2 did not induce obvious changes in the spectra, whereas the carbonate or bicarbonate species gradually decreased with H_2O and O_2 purging, indicating that the activated OH species also facilitated the decomposition of the carbonate or bicarbonate species.

On the basis of these results, we conclude that the addition of Na^+ ions did not change the reaction mechanism of the $Ir/TiO_2\text{-}R$ catalyst. Nevertheless, the $Na\text{-}Ir/TiO_2\text{-}R$ catalyst possessed much higher capacity for H_2O and O_2 activation than that of the $Ir/TiO_2\text{-}R$ catalyst because the formate species were consumed more rapidly by surface OH groups on the $Na\text{-}Ir/TiO_2$ catalyst.

4. CONCLUSIONS

In summary, this work demonstrated that Na addition has a dramatic promotion effect on Ir-based catalysts for ambient HCHO oxidation. Different from the $Na\text{-}Pt/TiO_2$ and $Na\text{-}Pd/TiO_2$ systems, Na addition to Ir/TiO_2 showed no much influence on Ir dispersion on the TiO_2 surface. Similarly, Na addition greatly facilitated the activation of both surface OH groups and chemisorbed oxygen, thus significantly increasing the activity of the Ir/TiO_2 catalyst. Furthermore, this study further demonstrates that alkali ions have a common promotion effect on noble metal-based catalysts for the HCHO oxidation reaction.

■ ASSOCIATED CONTENT

Supporting Information

The Supporting Information is available free of charge on the ACS Publications website at DOI: 10.1021/acscatal.8b03026.

HCHO conversions at different temperatures over the fresh Ir/TiO_2 and $Na\text{-}Ir/TiO_2$ samples, Ir dispersion calculation based on hemisphere model, and in situ DRIFTS spectra of $Ir/TiO_2\text{-}R$ and $Na\text{-}Ir/TiO_2\text{-}R$ catalysts (PDF)

■ AUTHOR INFORMATION

Corresponding Author

*E-mail: cbzhang@rcees.ac.cn.

ORCID

Changbin Zhang: 0000-0003-2124-0620

Author Contributions

⊥Y.L. and X.C. contributed equally to this work.

Notes

The authors declare no competing financial interest.

■ ACKNOWLEDGMENTS

This work was financially supported by the National Key R&D Program of China (2017YFC0211802) and National Natural Science Foundation of China (21577159, 21707136).

■ REFERENCES

(1) Tang, X. J.; Bai, Y.; Duong, A.; Smith, M. T.; Li, L. Y.; Zhang, L. P. Formaldehyde in China: Production, consumption, exposure levels, and health effects. *Environ. Int.* **2010**, *36*, 308−308.

(2) Maddalena, R.; Russell, M.; Sullivan, D. P.; Apte, M. G. Formaldehyde and Other Volatile Organic Chemical Emissions in Four FEMA Temporary Housing Units. *Environ. Sci. Technol.* **2009**, *43*, 5626−5632.

(3) Devoney, D.; Thompson, C. M.; Keshava, C.; Hsu, C. H.; Whalan, J. E. A critical review of the role of genotoxicity in formaldehyde-induced carcinogenicity: Relevance to public health. *Environ. Mol. Mutagen* **2006**, *47*, 445−445.

(4) Chang, M. B.; Lee, C. C. Destruction of Formaldehyde with Dielectric Barrier Discharge Plasmas. *Environ. Sci. Technol.* **1995**, *29*, 181−186.

(5) Rong, H. Q.; Liu, Z. Y.; Wu, Q. L.; Pan, D.; Zheng, J. T. Formaldehyde removal by Rayon-based activated carbon fibers modified by Paminobenzoic acid. *Cellulose* **2010**, *17*, 205−214.

(6) Moreno-Pirajan, J. C.; Tirano, J.; Salamanca, B.; Giraldo, L. Activated carbon modified with copper for adsorption of propanethiol. *Int. J. Mol. Sci.* **2010**, *11*, 927−42.

(7) Quiroz Torres, J.; Royer, S.; Bellat, J. P.; Giraudon, J. M.; Lamonier, J. F. Formaldehyde: catalytic oxidation as a promising soft way of elimination. *ChemSusChem* **2013**, *6*, 578−92.

(8) Shiraishi, F.; Ohkubo, D.; Toyoda, K.; Yamaguchi, S. Decomposition of gaseous formaldehyde in a photocatalytic reactor with a parallel array of light sources. *Chem. Eng. J.* **2005**, *114*, 153−159.

(9) Noguchi, T.; Fujishima, A.; Sawunyama, P.; Hashimoto, K. Photocatalytic Degradation of Gaseous Formaldehyde Using TiO_2 Film. *Environ. Sci. Technol.* **1998**, *32*, 3831−3833.

(10) Pei, J. J.; Zhang, J. S. Critical review of catalytic oxidization and chemisorption methods for indoor formaldehyde removal. *HVAC&R Res.* **2011**, *17*, 476−503.

(11) Wang, H. C.; Guo, W. Q.; Jiang, Z.; Yang, R. O.; Jiang, Z.; Pan, Y.; Shangguan, W. F. New insight into the enhanced activity of ordered mesoporous nickel oxide in formaldehyde catalytic oxidation reactions. *J. Catal.* **2018**, *361*, 370−383.

(12) Huang, Y. C.; Fan, W. J.; Long, B.; Li, H. B.; Qiu, W. T.; Zhao, F. Y.; Tong, Y. X.; Ji, H. B. Alkali-modified non-precious metal 3D-$NiCo_2O_4$ nanosheets for efficient formaldehyde oxidation at low temperature. *J. Mater. Chem. A* **2016**, *4*, 3648−3654.

(13) Hu, P. P.; Amghouz, Z.; Huang, Z. W.; Xu, F.; Chen, Y. X.; Tang, X. F. Surface-Confined Atomic Silver Centers Catalyzing Formaldehyde Oxidation. *Environ. Sci. Technol.* **2015**, *49*, 2384−2390.

(14) Tang, X. F.; Li, Y. G.; Huang, X. M.; Xu, Y. D.; Zhu, H. Q.; Wang, J. G.; Shen, W. J. MnO_x-CeO_2 mixed oxide catalysts for complete oxidation of formaldehyde: Effect of preparation method and calcination temperature. *Appl. Catal., B* **2006**, *62*, 265−273.

DOI: 10.1021/acscatal.8b03026
ACS Catal. 2018, 8, 11377−11385

(15) Tang, X. F.; Chen, J. L.; Li, Y. G.; Li, Y.; Xu, Y. D.; Shen, W. J. Complete oxidation of formaldehyde over Ag/MnO_x-CeO_2 catalysts. *Chem. Eng. J.* **2006**, *118*, 119−125.
(16) Qu, Z. P.; Shen, S. J.; Chen, D.; Wang, Y. Highly active Ag/SBA-15 catalyst using post-grafting method for formaldehyde oxidation. *J. Mol. Catal. A: Chem.* **2012**, *356*, 171−177.
(17) Huo, Y.; Wang, X. Y.; Rui, Z. B.; Yang, X. Q.; Ji, H. B. Identification of the Nearby Hydroxyls' Role in Promoting HCHO Oxidation over a Pt Catalyst. *Ind. Eng. Chem. Res.* **2018**, *57*, 8183−8189.
(18) Yang, T. F.; Huo, Y.; Liu, Y.; Rui, Z. B.; Ji, H. B. Efficient formaldehyde oxidation over nickel hydroxide promoted Pt/gamma-Al_2O_3 with a low Pt content. *Appl. Catal., B* **2017**, *200*, 543−551.
(19) Xu, Q.; Zhang, Y.; Mo, J.; Li, X. Indoor formaldehyde removal by thermal catalyst: kinetic characteristics, key parameters, and temperature influence. *Environ. Sci. Technol.* **2011**, *45*, 5754−60.
(20) Sekine, Y. Oxidative decomposition of formaldehyde by metal oxides at room temperature. *Atmos. Environ.* **2002**, *36*, 5543−5547.
(21) Li, Y.; Zhang, C.; Ma, J.; Chen, M.; Deng, H.; He, H. High temperature reduction dramatically promotes Pd/TiO_2 catalyst for ambient formaldehyde oxidation. *Appl. Catal., B* **2017**, *217*, 560−569.
(22) Zhang, C. B.; He, H. A comparative study of TiO_2 supported noble metal catalysts for the oxidation of formaldehyde at room temperature. *Catal. Today* **2007**, *126*, 345−350.
(23) Kim, S. S.; Park, K. H.; Hong, S. C. A study on HCHO oxidation characteristics at room temperature using a Pt/TiO_2 catalyst. *Appl. Catal., A* **2011**, *398*, 96−103.
(24) Imamura, S.; Uematsu, Y.; Utani, K.; Ito, T. Combustion of formaldehyde on ruthenium/cerium (IV) oxide catalyst. *Ind. Eng. Chem. Res.* **1991**, *30*, 18−21.
(25) Huang, H. B.; Leung, D. Y. C. Complete Oxidation of Formaldehyde at Room Temperature Using TiO_2 Supported Metallic Pd Nanoparticles. *ACS Catal.* **2011**, *1*, 348−354.
(26) Li, H. F.; Zhang, N.; Chen, P.; Luo, M. F.; Lu, J. Q. High surface area Au/CeO_2 catalysts for low temperature formaldehyde oxidation. *Appl. Catal., B* **2011**, *110*, 279−285.
(27) Xu, J.; Qu, Z.; Wang, Y.; Huang, B. HCHO oxidation over highly dispersed Au nanoparticles supported on mesoporous silica with superior activity and stability. *Catal. Today* **2018**, in press DOI: 10.1016/j.cattod.2018.04.051.
(28) Zhang, C. B.; He, H.; Tanaka, K.-i. Catalytic performance and mechanism of a Pt/TiO_2 catalyst for the oxidation of formaldehyde at room temperature. *Appl. Catal., B* **2006**, *65*, 37−43.
(29) Zhang, C. B.; Liu, F. D.; Zhai, Y. P.; Ariga, H.; Yi, N.; Liu, Y. C.; Asakura, K.; Flytzani-Stephanopoulos, M.; He, H. Alkali-Metal-Promoted Pt/TiO_2 Opens a More Efficient Pathway to Formaldehyde Oxidation at Ambient Temperatures. *Angew. Chem., Int. Ed.* **2012**, *51*, 9628−9632.
(30) Zhang, C. B.; He, H.; Tanaka, K.-i. Perfect catalytic oxidation of formaldehyde over a Pt/TiO_2 catalyst at room temperature. *Catal. Commun.* **2005**, *6*, 211−214.
(31) Zhang, C. B.; Li, Y. B.; Wang, Y. F.; He, H. Sodium-Promoted Pd/TiO_2 for Catalytic Oxidation of Formaldehyde at Ambient Temperature. *Environ. Sci. Technol.* **2014**, *48*, 5816−5822.
(32) Bai, B. Y.; Li, J. H. Positive Effects of K^+ Ions on Three-Dimensional Mesoporous Ag/Co_3O_4 Catalyst for HCHO Oxidation. *ACS Catal.* **2014**, *4*, 2753−2762.
(33) Chen, Y. X.; Gao, J. Y.; Huang, Z. W.; Zhou, M. J.; Chen, J. X.; Li, C.; Ma, Z.; Chen, J. M.; Tang, X. F. Sodium Rivals Silver as Single-Atom Active Centers for Catalyzing Abatement of Formaldehyde. *Environ. Sci. Technol.* **2017**, *51*, 7084−7090.
(34) Siang, J. Y.; Lee, C. C.; Wang, C. H.; Wang, W. T.; Deng, C. Y.; Yeh, C. T.; Wang, C. B. Hydrogen production from steam reforming of ethanol using a ceria-supported iridium catalyst: Effect of different ceria supports. *Int. J. Hydrogen Energy* **2010**, *35*, 3456−3462.
(35) Bi, Q. Y.; Du, X. L.; Liu, Y. M.; Cao, Y.; He, H. Y.; Fan, K. N. Efficient Subnanometric Gold-Catalyzed Hydrogen Generation via Formic Acid Decomposition under Ambient Conditions. *J. Am. Chem. Soc.* **2012**, *134*, 8926−8933.
(36) Sato, Y.; Soma, Y.; Miyao, T.; Naito, S. The water-gas-shift reaction over Ir/TiO_2 and Ir-Re/TiO_2 catalysts. *Appl. Catal., A* **2006**, *304*, 78−85.
(37) Liotta, L. F.; Deganello, G.; Delichere, P.; Leclercq, C.; Martin, G. A. Localization of alkali metal ions in sodium-promoted palladium catalysts as studied by low energy ion scattering and transmission electron microscopy. *J. Catal.* **1996**, *164*, 334−340.
(38) Liotta, L. F.; Martin, G. A.; Deganello, G. The Influence of Alkali Metal Ions in the Chemisorption of CO and CO_2 on Supported Palladium Catalysts: A Fourier Transform Infrared Spectroscopic Study. *J. Catal.* **1996**, *164*, 322−333.
(39) Panagiotopoulou, P.; Kondarides, D. I. Effects of alkali promotion of TiO_2 on the chemisorptive properties and water−gas shift activity of supported noble metal catalysts. *J. Catal.* **2009**, *267*, 57−66.
(40) Onishi, H.; Aruga, T.; Egawa, C.; Iwasawa, Y. Modification of Surface Electronic-Structure on TiO_2 (110) and TiO_2 (441) by Na Deposition. *Surf. Sci.* **1988**, *199*, 54−66.
(41) Nie, L. H.; Yu, J. G.; Li, X. Y.; Cheng, B.; Liu, G.; Jaroniec, M. Enhanced performance of NaOH-modified Pt/TiO_2 toward room temperature selective oxidation of formaldehyde. *Environ. Sci. Technol.* **2013**, *47*, 2777−83.
(42) Brookes, I.; Muryn, C.; Thornton, G. Imaging Water Dissociation on TiO_2 (110). *Phys. Rev. Lett.* **2001**, *87*, 1−4.
(43) Zhai, Y. P.; Pierre, D.; Si, R.; Deng, W.; Ferrin, P.; Nilekar, A. U.; Peng, G. W.; Herron, J. A.; Bell, D. C.; Saltsburg, H.; Mavrikakis, M.; Flytzani-Stephanopoulos, M. Alkali-stabilized Pt-OHx species catalyze low-temperature water-gas shift reactions. *Science* **2010**, *329*, 1633−6.
(44) Wang, X.; Rui, Z.; Ji, H. DFT study of formaldehyde oxidation on silver cluster by active oxygen and hydroxyl groups: Mechanism comparison and synergistic effect. *Catal. Today* **2018**, in press DOI: 10.1016/j.cattod.2018.06.021.
(45) Li, S.; Lu, X.; Guo, W.; Zhu, H.; Li, M.; Zhao, L.; Li, Y.; Shan, H. Formaldehyde oxidation on the Pt/TiO_2(101) surface: A DFT investigation. *J. Organomet. Chem.* **2012**, *704*, 38−48.
(46) Zhang, Z.; Bondarchuk, O.; Kay, B. D.; White, J. M.; Dohnalek, Z. Imaging water dissociation on TiO_2 (110): Evidence for inequivalent geminate OH groups. *J. Phys. Chem. B* **2006**, *110*, 21840−21845.
(47) Vecchietti, J.; Bonivardi, A.; Xu, W. Q.; Stacchiola, D.; Delgado, J. J.; Calatayud, M.; Collins, S. E. Understanding the Role of Oxygen Vacancies in the Water Gas Shift Reaction on Ceria-Supported Platinum Catalysts. *ACS Catal.* **2014**, *4*, 2088−2096.
(48) Ojifinni, R. A.; Froemming, N. S.; Gong, J.; Pan, M.; Kim, T. S.; White, J. M.; Henkelman, G.; Mullins, C. B. Water-Enhanced Low-Temperature CO Oxidation and Isotope Effects on Atomic Oxygen-Covered Au(111). *J. Am. Chem. Soc.* **2008**, *130*, 6801−6812.
(49) Bongiorno, A.; Landman, U. Water-enhanced catalysis of CO oxidation on free and supported gold nanoclusters. *Phys. Rev. Lett.* **2005**, *95*, 1−4.
(50) Kim, T. S.; Gong, J.; Ojifinni, R. A.; White, J. M.; Mullins, C. B. Water Activated by Atomic Oxygen on Au(111) to Oxidize CO at Low Temperatures. *J. Am. Chem. Soc.* **2006**, *128*, 6282−6283.
(51) Liu, L. M.; McAllister, B.; Ye, H. Q.; Hu, P. Identifying an O_2 supply pathway in CO oxidation on Au/TiO_2 (110): A density functional theory study on the intrinsic role of water. *J. Am. Chem. Soc.* **2006**, *128*, 4017−4022.
(52) Ammal, S. C.; Heyden, A. Water-Gas Shift Catalysis at Corner Atoms of Pt Clusters in Contact with a TiO_2 (110) Support Surface. *ACS Catal.* **2014**, *4*, 3654−3662.

DOI: 10.1021/acscatal.8b03026
ACS Catal. 2018, 8, 11377−11385